Model for Blast Waves of Boiling Liquid Expanding Vapor Explosions[☆,☆☆]

S. E. Yakush

Institute for Problems in Mechanics of the Russian Academy of Sciences, Ave. Vernadskogo 101 Bldg 1, Moscow, 119526, Russia

Abstract

A numerical model for boil-up of superheated liquid following loss of containment and expansion of two-phase mixture into the atmosphere is proposed and applied to evaluation of blast effects of Boiling Liquid Expanding Vapor Explosions (BLEVEs). The model assumes that the mixture in the two-phase cloud stays in thermodynamic equilibrium during expansion, whereas the air in the atmosphere obeys the ideal gas law with constant ratio of specific heats. The boundary between the two-phase cloud and ambient atmosphere is considered as a moving contact surface. The problem is solved numerically in the axisymmetric framework. Sample calculations of expansion of a spherical volume of superheated liquid are carried out for pressure-liquefied propane. Pressure profiles demonstrating propagation of depressurization wave into the cloud are presented together with mass fractions of vapor in the mixture. Solutions obtained for two-phase systems are compared with those for single-phase compressed gas. Scaling of overpressures in physical explosions is discussed. Validation of the model is carried out by comparison of simulations carried out in a wide range of cloud masses with experimental data. Two-dimensional simulations demonstrating BLEVE blast waves from a bursting near-surface vessel are presented.

Keywords: BLEVE, Blast wave, Overpressure, Thermal equilibrium model, Numerical modeling

1. Introduction

Accidental releases of pressurized or pressure-liquefied substances are one of major hazards in process industries, transportation or storage of flammable materials. Such releases can be caused by bursts of high-pressure vessels, pipeline rupture, processing equipment malfunction etc [1]. Some striking examples of how destructive the explosions caused by accidental releases of flammable substances into the atmosphere can be are the accidents in Port Hudson (USA, 1970), Flixborough (UK, 1974), Mexico City (Mexico, 1984), Ufa (Russia, 1989), Xian (China, 1998), Nechapur (Iran, 2004), Buncefield (UK, 2005).

In the conventional explosions, rapid combustion or detonation of fuel yields the energy causing expansion of combustion products which act as a piston driving the ambient gas. However, there are different kinds of explosions, termed as "physical" (rather than chemical), which are driven by the internal energy accumulated in compressed gas or superheated liquid [2]. A well-known example of such an explosion is the burst of a vessel with pressure-liquefied substance, known as Boiling Liquid Expanding Vapor Explosion (BLEVE) [3, 4]. BLEVE-type events, though occurring typically with pressure-liquefied hydrocarbons, can also occur with non-flammable substances, or even water, provided that preheating of vessel is high enough to bring the substance to the superheated state with respect to its thermodynamic equilibrium state at the ambient pressure.

It has been shown experimentally that parameters of shock waves from physical explosions differ substantially from those of TNT blasts [2, 5, 6]. Large and medium-scale tests on physical explosions and BLEVEs are quite rare [7, 8, 9, 10]; laboratory-scale experiments [11, 12, 2, 5, 6] play an important role for understanding the features of shock waves generated by expanding superheated liquids, but there remains uncertainty on how to scale the results up to real accidents, keeping in mind multiple length and time scales present in the problem. Therefore, mathematical modeling is helpful in filling this gap.

Several BLEVE blast models have been proposed so far, differing in the assumptions and level of detail with which the complicated transient multiphase processes involved are tackled [13, 14, 15, 16, 17, 18, 19, 20]. The approaches can be classified into the following broad categories: i) empirical correlations aiming at comparing the BLEVE blast wave characteristics (overpressure, impulse) with those of high explosives (TNT equivalence approach) [18, 19, 10, 20]; ii) models focusing on the processes of liquid boil-up, superheat temperature limit, nucleation in superheated liquid, bubble growth etc. [21, 22, 23, 24]; iii) gas-dynamical models focusing on blast wave propagation in the atmosphere, while simplifying the description of boil-up processes by the assumption of expansion-controlled evaporation [16] or by approximating the expanding two-phase mixture by an equivalent gas [19]. The purpose of this work is to develop and validate a model "balanced" with respect to the details level of the "internal" or "external" problems.

The proposed model for expansion of a volume of superheated liquid is based upon the assumption that, as the pressure decreases, the liquid boils up and evaporates, this process be-

[☆☆]DOI: http://dx.doi.org/10.1016/j.ijheatmasstransfer.2016.07.048

Email address: yakush@ipmnet.ru (S. E. Yakush)

URL: http://www.ipmnet.ru/~yakush/en (S. E. Yakush)

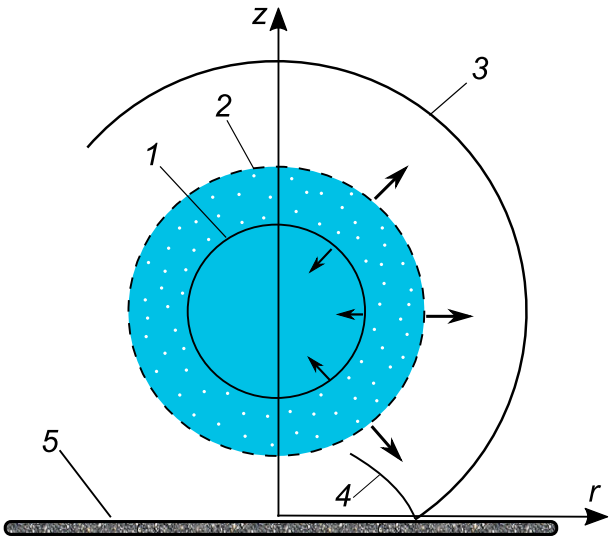

Figure 1: Sketch of a superheated liquid cloud expanding into the atmosphere: *1* — boiling front, *2* — outer boundary of expanding two-phase cloud, *3* — atmospheric blast wave, *4* — reflected shock, *5* — ground surface

ing fast enough in comparison with the characteristic expansion time so that the vapor/liquid mixture reaches thermodynamic equilibrium. A similar model was applied to depressurization of ruptured pipes [25]; the difference is that an open atmosphere is considered, and no interaction with walls or flow choking occur. Another assumption is that no mixing occurs on the boundary between the expanding superheated liquid and ambient gas.

In what follows, mathematical model and its numerical implementation are presented, then spherical cloud expansion is considered, focusing on scaling of BLEVE overpressures with liquid mass and initial pressure. Finally, results of near-ground BLEVE simulations are validated against the experimental data.

2. Mathematical model

The assumed structure of superheated liquid expansion in the atmosphere is presented in Fig. 1. Two distinct zones are considered: i) inner zone which includes the superheated liquid and thermodynamically equilibrium two-phase mixture emerging upon its boil-up, and ii) ambient atmosphere in which shock waves can be generated by piston action of the expanding cloud.

The mathematical model describing the inner zone includes the continuity and momentum equations for boiling liquid-vapor mixture:

$$\frac{\partial \rho_m}{\partial t} + \nabla \rho_m U_m = 0, \tag{1}$$

$$\frac{\partial \rho_m U_m}{\partial t} + \nabla \rho_m U_m \otimes U_m = -\nabla P. \tag{2}$$

The mixture density, ρ_m, is obtained from specific volumes of liquid (subscript l) and vapor (subscript v), and mass fraction of vapor x_v:

$$\rho_m = \frac{1}{(1-x_v)\, v_l^0 + x_v v_v^0} \tag{3}$$

The specific volumes of both phases, $v_{l,v}^0$, are taken on the saturation line at the local pressure P, while x_v is evaluated from the isoentropic relation

$$s_l^0(P_0) = (1-x_v)\, s_l^0(P) + x_v s_v^0(P), \tag{4}$$

with the liquid and vapor entropies, $s_{l,v}^0$, also taken on the saturation line. The mixture equation of state (3) is barotropic (ρ_m is a unique function of P). However, since s_l^0 depends on the initial pressure P_0 (see Eq. (4)), the mass fraction of vapor depends on both P and P_0:

$$x_v(P, P_0) = \frac{s_l^0(P_0) - s_l^0(P)}{s_v^0(P) - s_l^0(P)}. \tag{5}$$

Therefore, the mixture density also depends on P_0 parametrically: $\rho_m = \rho_m(P, P_0)$.

The equation of state for two-phase mixture, Eqs. (3) and (4), is only valid for $P \le P_0$, which is generally sufficient for the description of the initial stage of two-phase mixture expansion into lower-pressure atmosphere. However, it will be shown later on that converging shock waves can be formed in the mixture leading to implosion causing short-duration peak pressures at the cloud center exceeding P_0. Therefore, the equation of state must be extended to pressures $P > P_0$ where the single-phase liquid becomes subcooled with respect to its saturation temperature at the local pressure. It was assumed that compression of single-phase liquid is isothermal (proceeding at the saturation temperature corresponding to P_0), and the pressure-density relationship is described by the modified Tait equation [26]

$$P = P_0 + B\left(\left(\frac{\rho_m}{\rho_0}\right)^n - 1\right) \tag{6}$$

where ρ_0 is the density of saturated liquid at $P = P_0$. In the subcooled liquid, we set $x_v(P, P_0) = 0$, so that the mixture density and mass fraction of vapor are continuous on the saturation line dividing the saturated mixture and subcooled compressed liquid. However, the speed of sound is discontinuous; in the subcooled liquid it is calculated from (6) as

$$C_s = \left(\frac{dP}{d\rho_m}\right)^{1/2} = \left(\frac{nB\left(\frac{\rho_m}{\rho_0}\right)^n}{\rho_m}\right)^{1/2} \tag{7}$$

Equation (6) is also barotropic, so that the same numerical procedure can be applied for solving the mixture continuity and momentum equations in the whole two-phase zone. The Tait equation (6) describes compression of liquid from its saturated state, i. e., the reference density $\rho_0 = \rho_{sat}(P_0)$ and parameters B, n depend on P_0 (increase in P_0 means increase in the saturation temperature T_0, decrease in ρ_0, and increase in liquid compressibility).

In the ambient atmosphere, the Euler equations are solved, with the air considered as an ideal gas with the ratio of specific heats $\gamma = 1.4$. The boundary between the zones is a contact surface moving with time. The pressure and normal velocity component are continuous across the contact surface, whose shape and position are obtained in the course of the solution.

A similar model was applied earlier to spherically symmetric expansion of superheated liquids [13, 14, 15]. Here, the model is extended to multidimensional problems, so that it is applicable to near-ground vessel explosions.

3. Numerical method

The complex problem requiring solution of different equation sets in different domains divided by a sharp contact interface is tackled by the Ghost Fluid Method (GFM) [27] in which the cells neighboring the interface are alternatively filled with "ghost" fluid of the same type as current, enabling solution of equations across the boundary. The sharp interface is considered as a moving level-set $\phi = 0$ of the distance function for which the evolution equation is solved [28]:

$$\frac{\partial \phi}{\partial t} + U \cdot \nabla \phi = 0. \qquad (8)$$

To resolve the sharp gradients without smearing the solution due to numerical diffusion, high-order central difference scheme with the flux limiters maintaining non-oscillatory behavior [29] was applied in each subdomain to solve the governing equations.

The program was implemented in FORTRAN-90, with the possibility to switch between 2D (axially symmetric) and 1D (spherically symmetric) geometries. The latter case allowed us to run simulations on fairly fine grids (10^4 cells in 1D), while 2D simulations were run on 500×500 grids. In the one-dimensional case, convergence of solutions with respect to grid size was checked by running test cases with grid cell sizes increased by the factor of 2 and 5. The radial positions of shock wave fronts and pressure profiles between shocks coincided well within 1% for all three grids. The shocks fronts were smeared by numerical scheme to about four grid cells on each grid; importantly, this did not affect the predicted overpressures. In the two-dimensional case, simulations were repeated on the same grid, but in larger computational domains, necessary to obtain the overpressure-distance data. It was found that, despite lower resolution in the two-phase cloud region, the shock wave overpressure was not very sensitive to the grid size.

4. Properties of Two-phase Equilibrium Mixture

The model for thermodynamically equilibrium mixture requires properties of each phase on the saturation line; these were taken from the NIST data tables [30]. Before resorting to the results obtained in numerical simulations, consider the physical properties of two-phase mixture described by Eqs. (3)–(5).

In Fig. 2, pressure dependencies of the vapor mass fraction x_v and mixture density ρ_m are plotted for propane at three different initial pressures $P_0 = 5$, 10, and 20 bar. Evidently, the mixture density is a substantially non-linear function of pressure, in sharp contrast to linear dependencies typical of isothermal compression of each individual phase. Also, upon adiabatic compression of an ideal gas with some ratio of specific heats

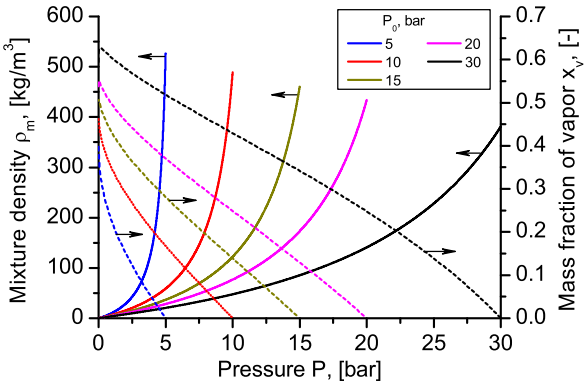

Figure 2: Density ρ_m (solid lines) and mass fraction of vapor x_v (dashed lines) for equilibrium two-phase propane liquid-vapor mixture at different initial pressures P_0

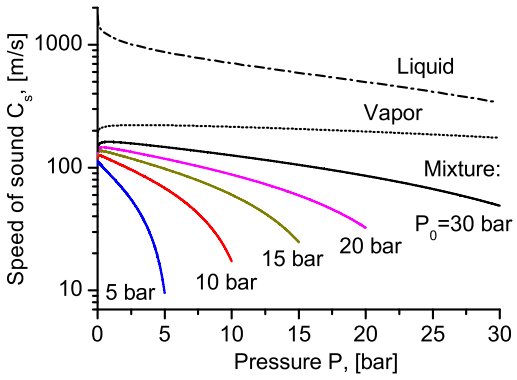

Figure 3: Effective speed of sound in equilibrium two-phase propane liquid-vapor mixture (solid lines) in comparison with the speed of sound in single-phase saturated liquid (dash-dotted line) and vapor (dashed line)

$\gamma > 1$, the curve describing the density as a function of pressure, $\rho \propto P^{1/\gamma}$, is convex upward, whereas the density curves in Fig. 2 are convex downward. Therefore, it is very problematic to approximate the two-phase mixture by some "equivalent" ideal gas which would allow the well-known shock tube relationships to be applied.

Thermodynamically equilibrium two-phase mixture is characterized by very high effective compressibility (until the limit of single-phase liquid is reached) which exceeds by far compressibility of each individual phase (vapor and liquid). Such high compressibility is due to the fact that pressure changes lead mainly to evaporation or condensation of substance (variation of x_v, see Eq. (5)), rather than to compression of each phase. Note that the assumption of thermodynamic equilibrium means instantaneous adjustment of mixture density to pressure, i. e., evaporation/condensation rate is not a limiting factor. As a result, the equilibrium two-phase mixture possesses low isoentropic speed of sound $C_s = (\partial\rho_m/\partial P)_s^{-1/2}$. The effective speed of sound in the two-phase propane obtained by differentiating Eqs. (3) and (5) is plotted against pressure in Fig. 3 at the same three initial pressures $P_0 = 5$, 10, and 20 bar as in Fig. 2. Also, the speeds of sound in single-phase vapor and liquid are plotted. One can see that sound of speed in two-phase mixture depends strongly upon pressure, it is significantly lower that the typical speed of sound in liquids (of the order of 1000 m/s) and gases (of the order of 300 m/s).

If follows from Figs. 2 and 3 that the boiling-up front separates two substances with very different properties, a liquid and two-phase mixture. The low speed of sound on the two-phase side is a physical reason which limits the rate at which pressure drop penetrates into the volume of superheated liquid. This, in turn, limits the internal energy release rate.

The energy yield per unit mass of pressure-liquefied gas is obtained as the difference of specific enthalpies of the initial (superheated) liquid and equilibrium two-phase mixture in its final state (at the atmospheric pressure):

$$\Delta h_{lv} = h_l^0(P_0) - \left\{(1 - x_v)\, h_l^0(P_a) + x_v h_v^0(P_a)\right\}. \qquad (9)$$

where $x_v = x_v(P_0, P_a)$ is the mass fraction of vapor determined by Eq. (5), the specific enthalpies of both phases $h_{l,v}^0$ are taken on the saturation curve at the corresponding pressures.

Equation (9) allows us to estimate the characteristic velocity of the mixture:

$$U_* = (2\Delta h_{lv})^{1/2}. \qquad (10)$$

In Table 1, results are obtained for evaporation of $M = 10^3$ kg of pressure-liquefied propane at various initial pressures and corresponding saturation temperatures. The total energy released, $E = M\Delta h_{lv}$, is given in the energy units, as well as in TNT equivalent units (1 kg TNT is 4.184 MJ). Note that this conversion to TNT units is performed only to demonstrate more clearly the significant amount of internal energy stored in the superheated liquid, it is not assumed that pressure waves generated in the atmosphere are comparable. Noteworthy, the characteristic expansion velocities U_* calculated from (10) are close to the speed of sound in atmosphere, and with initial preheating even exceed it. This high expansion velocity is responsible for generation of atmospheric shock waves in the events of BLEVE.

Table 1: Energy characteristics of explosive boil-up of 1 tonne of propane

P_0, bar	T_0, K	x_v, %	E, MJ	TNT, kg	U_*, m/s
5	275.3	22.4	9.8	2.3	138.7
10	300.6	34.8	23.8	5.7	216.4
15	317.1	42.9	36.4	8.7	269.8
20	330.4	49.8	49.5	11.8	312.5
25	341.4	55.2	61.0	14.6	349.3
30	351.5	60.8	74.3	17.8	382.8

No ready-to-use relationships for the parameters B and n of Tait equation (6) were found in the literature for the substances of interest in the current study (note that these parameters must describe compressibility in the wide range of pressures starting from the saturated state, whereas most values found were relevant to liquids well below their saturation point). Therefore, data from the NIST tables [30] (based on the model [31]) were used for several initial pressures P_0; the dependencies of liquid density on pressure were processed in the range from P_0 to the maximum pressure of 500 bar, and best fit parameters B and n were found in each case. It was found that it is possible to approximate all data with a single value of power exponent n, and B can be approximated by the power-law function of saturation density ρ_0 (which is a function of saturation pressure P_0). For propane in the range of $P_0 = 5 - 30$ bar the best fit is achieved for $n = 9$ and $B = 264.4\,(\rho_0/100)^7$ Pa.

5. Results

5.1. Structure of expanding spherical cloud of superheated liquid

Consider first the results obtained for spherically symmetric expansion of pressure-liquefied propane, focusing on the structure of the cloud and pressure profiles in the two-phase zone and in the atmosphere. To this end, three cases are considered below, with the vessel diameter of 1 m and initial pressure $P_0 = 5$, 15, and 25 bar (corresponding to the initial temperatures of $T_0 = 274.9$, 317.1, 341.4 K and initial densities of $\rho_0 = 526.3$, 460.3, and 408.3 kg/m^3). Note that higher initial pressures correspond to lower densities of saturated liquid due to higher saturation temperatures. At these conditions, the masses of propane for the volume of $V = 0.524$ m^3 are $M = 275.6$, 241.2, and 213.8 kg, whereas the total internal energies stored in superheated liquid are 2.65, 8.78, and 13.0 MJ, respectively, the energy-based characteristic velocities evaluated according to (10) are 138.7, 269.8, and 349.3 m/s.

Numerical simulations were carried out in spherical symmetry on a grid spanning the radius 0–50 m, with 10^4 cells, so that the cell size was as little as 5 mm.

In Fig. 4, the pressure profiles (top row) and mass fraction of vapor (bottom) are shown at different times, demonstrating the expansion process at the initial pressure $P_0 = 5$ bar. The open dot symbol on each pressure profile denotes the position

of contact surface between the two-phase liquid/vapor mixture and air, corresponding to the rightmost boundary of non-zero mass fraction of vapor on the $x_v(r)$ graphs.

Cloud expansion proceeds in two distinct stages. The first one, lasting for the specified initial conditions up to $t = 25$ ms, is presented in the left column of Fig. 4. This stage is featured by layer-by-layer boil-up of superheated cloud and expansion of the two-phase mixture, giving rise to the shock wave propagating in the atmosphere. This rapidly propagating blast wave is visible in Fig. 4 only on the pressure profiles corresponding to the times up to $t = 5$ ms, then the shock leaves the domain plotted. Properties of this air shock (including the overpressure decay with distance) will be considered in Section 5.3; here we focus on the analysis of two-phase cloud size and structure.

A distinct feature of the pressure profiles is the development of low pressures in the two-phase zone behind the contact surface. By the time $t = 10$ ms a backward-facing secondary shock is formed in the cloud; up to the time $t = 25$ ms this shock moves outwards, together with the contact surface. These results agree qualitatively with observations [19] where overexpansion to sub-atmospheric pressures behind the contact surface was observed experimentally.

At time $t = 25$ ms, cloud expansion rapidly slows down, the two-phase cloud reaches its maximum size of about 2 m (in radius), after which the second stage (cloud contraction) begins. As can be seen in the right column of Fig. 4, the inward-facing shock propagates towards the cloud center, converging and causing implosion at about $t = 48$ ms. The pressure surge due to implosion results in vapor condensation in the cloud center (it is at this stage the single-phase equation of state (6) becomes necessary in the model), and the reflected secondary blast wave starts to propagate outwards. This wave is much weaker than the primary atmospheric shock, however, it can explain the double-peak pressure records obtained experimentally.

Further evolution of the two-phase cloud exhibits weaker pressure waves, it is not considered here mostly because at large times turbulent mixing of the cloud and ambient air must become the primary mechanism governing the growth of two-phase cloud and further evaporation of droplets. Effects of turbulence mixing, though, were not taken into account in the BLEVE model developed in this work (see [14] for a model of fuel cloud turbulent growth following pressure vessel bursts).

In Figs. 5 and 6, results obtained for higher initial pressures $P_0 = 15$ and 25 bar are plotted. Comparison of these figures with Fig. 4 shows that the two-stage process of superheated cloud expansion is also observed for higher superheat. However, there are several distinct features in each case. The higher the initial pressure, the more rapid is expansion process. In the two cases under consideration, the time at which the inward-facing shock and contact surface turn from expansion to compression is equal to $t = 18$ ms and $t = 15$ ms, as opposed to $t = 25$ ms in Fig. 4. By this time, the boil-up front travels only half the initial cloud radius in the case of $P_0 = 5$ bar, whereas it just reaches the cloud center in the case of $P_0 = 15$ bar. In the case of $P_0 = 25$ bar, total boil-up of all superheated liquid occurs at $t = 11$ ms, i. e., earlier than cloud expansion stops.

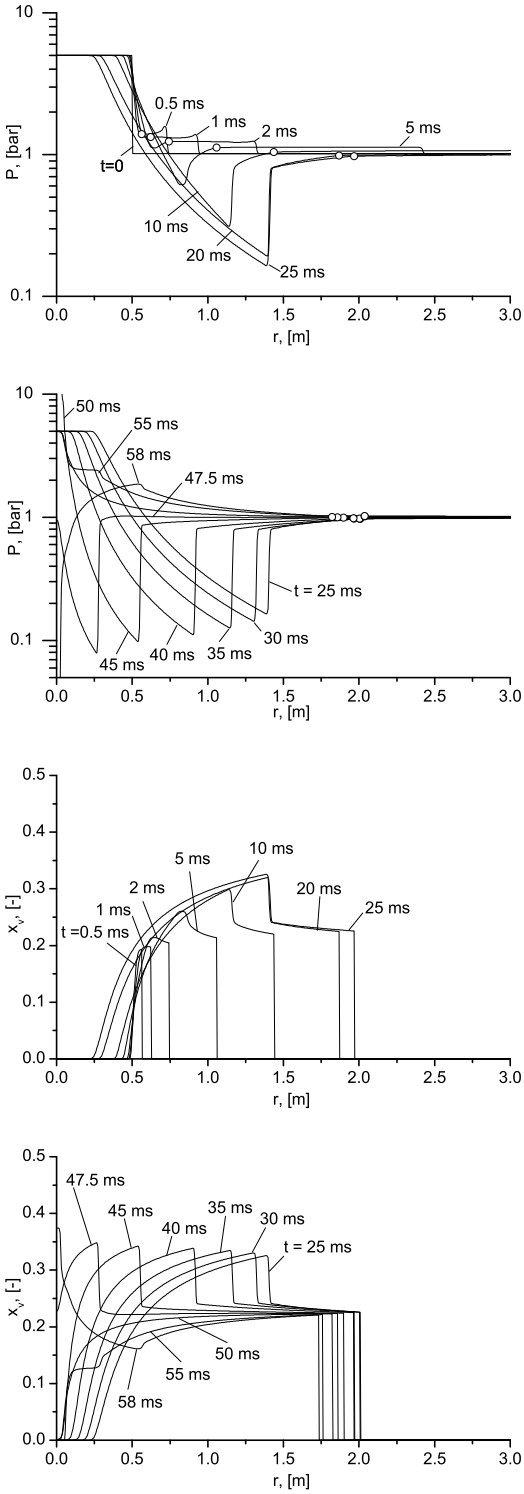

Figure 4: Pressure (top row) and vapor mass fraction (bottom row) profiles in expanding propane cloud, $P_0 = 5$ bar. Symbols denote positions of the contact surface

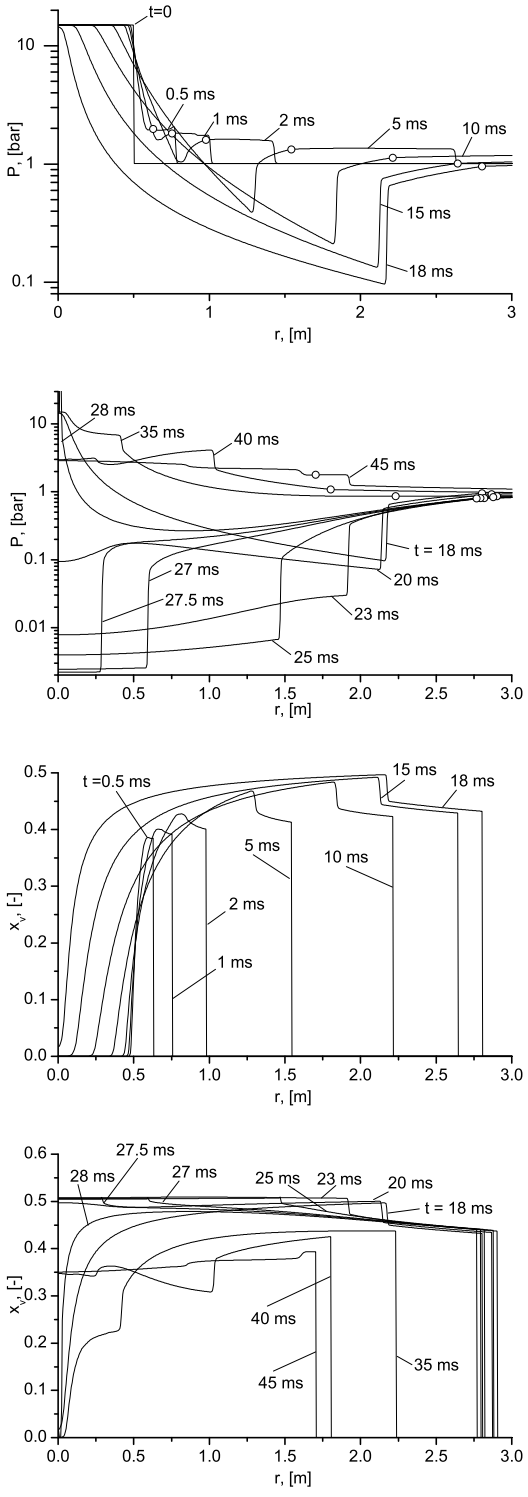

Figure 5: Pressure (top row) and vapor mass fraction (bottom row) profiles in expanding propane cloud, P_0 = 15 bar

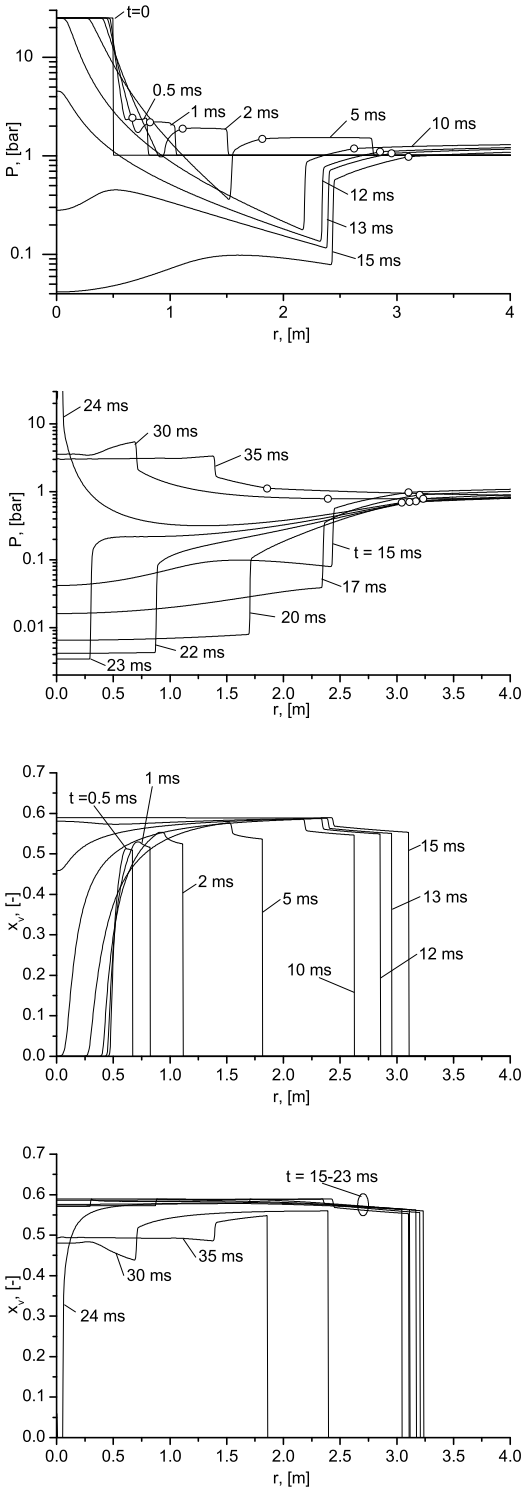

Figure 6: Pressure (top row) and vapor mass fraction (bottom row) profiles in expanding propane cloud, P_0 = 25 bar

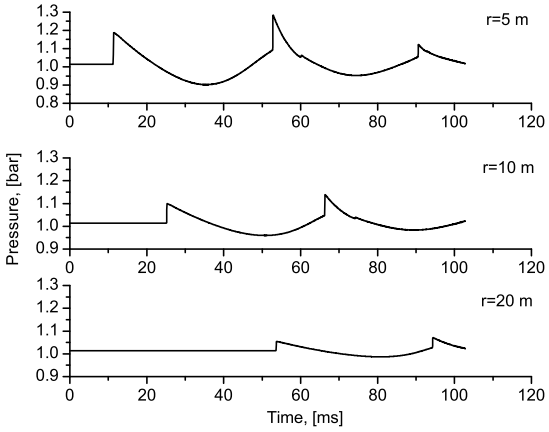

Figure 7: Time profiles of pressure at different distances from the cloud center, P_0 = 15 bar

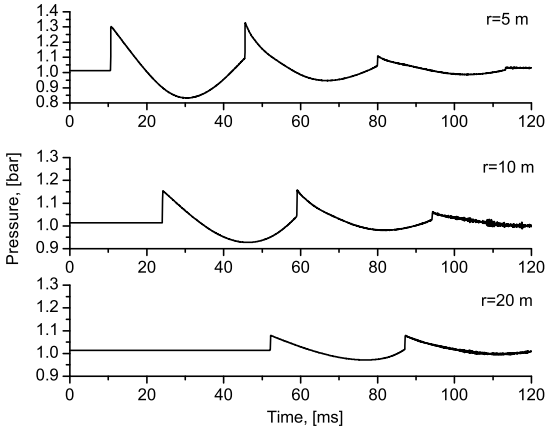

Figure 8: Time profiles of pressure at different distances from the cloud center, P_0 = 25 bar

The maximum radius reached by the two-phase cloud is 2.0, 2.9, and 3.25 m, respectively.

The shape of pressure pulse at several distances from the burst point can be seen in Figures 7 (for P_0 = 15 bar) and 8 (for P_0 = 25 bar), where pressure time histories are presented at the distances of 5, 10, and 20 m from the explosion point (cloud center). Two to three pressure peaks are clearly seen, corresponding to the arrival of the primary, as well as reflected pressure waves. These results agree with experimental observations where multiple shocks were recorded in BLEVE blasts [19].

5.2. Boiling wave properties

Figures 4–6 show the boiling wave propagating in the superheated liquid towards the center. It is of interest to obtain some quantitative properties of this wave, providing insight into the complex processes involved in BLEVEs. To this end, results of simulations carried out for vessel of 1 m diameter and different initial pressures were processed: position r_b of the boiling front was determined from the profiles of vapor mass fraction $x_v(r)$,

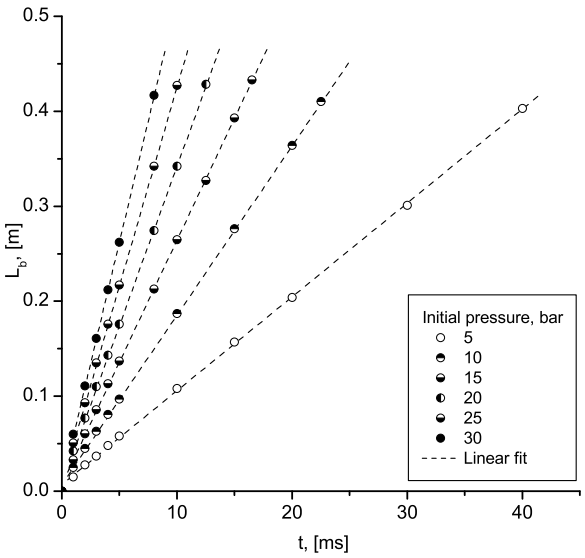

Figure 9: Distance traveled by boiling front L_b vs time t; dashed lines show data fit by linear functions

and the distance traveled by the boiling wave $L_b = r_0 - r_b$ was plotted as a function of time, see Fig. 9. At all initial pressures the boiling front propagates with constant velocity U_b which was found by fitting the data by linear functions. The velocities obtained numerically coincide within 3% accuracy with the speed of sound in the two-phase mixture C_s at the initial pressure P_0, evaluated as was described in Section 4. Numerical values for both velocities are presented in Table 2 for the range of initial pressures in question. Since the boiling front is propagating through non-moving saturated liquid, it is possible to evaluate the mass flux $G_b = \rho_l^0 U_b$, i. e., mass of liquid passing through a unit area of the boiling front per unit time (here, ρ_l^0 is the saturated liquid density at P_0, also listed in Table 2. Note that liquid crossing the boiling front evaporates not immediately, but gradually, as its pressure is diminished due to cloud expansion.

Table 2: Boiling wave properties

P_0, bar	ρ_l^0, kg/m^3	C_s, m/s	U_b, m/s	G_b, kg/m^{2}s
5	526.3	9.54	9.88	$5.20 \cdot 10^3$
10	489.3	17.29	17.82	$8.72 \cdot 10^3$
15	460.3	24.77	25.70	$11.83 \cdot 10^3$
20	434.1	32.33	33.48	$14.53 \cdot 10^3$
25	408.3	40.26	41.79	$17.06 \cdot 10^3$
30	381.2	48.88	51.00	$19.44 \cdot 10^3$

5.3. Scaling of BLEVE blast wave overpressures

A common approach to generalization of blast wave results (theoretical or experimental) is Sachs's scaling in which

non-dimensional overpressure $\overline{\Delta P} = (P_{\max} - P_a)/P_a$ is plotted against the reduced distance $\bar{r} = r/r_*$, with the length scale $r_* = (E/P_a)^{1/3}$ based on the explosion energy yield E.

This approach proves successful for high explosives because the source sizes are very small and the energy is release is nearly instantaneous, so that no intrinsic length and time scales except those based on the total energy appear in the problem. For physical explosions, neither of these factors is strictly true. In this section, we apply the energy-based scaling approach to the (numerically generated) BLEVE blast waves, considering the effects of superheated liquid mass and initial pressure, all affecting the explosion yield $E = M \cdot \Delta h_{lv}$ (see Eq. (9). We consider here spherically symmetric expansion of superheated propane in an unbounded atmosphere, paying particular attention to the properties of blast waves propagating in the air. The simulation results are processed in Sachs's coordinates and compared with well-known overpressure-distance dependencies for TNT.

5.3.1. Effect of cloud mass at a fixed initial pressure

In the idealized case of spherically symmetric expansion of superheated liquid in an infinite atmosphere, it can be shown that for the same substance and fixed initial pressure the solutions obtained for different masses must coincide in relevant non-dimensional coordinates. Indeed, the specific energy yield, Δh_{lv}, and, therefore, the characteristic velocity $U_* = \sqrt{2\Delta h_{lv}}$ are constant, while the energy-based length scale $r_* = (E/P_a)^{1/3} = (M \cdot \Delta h_{lv}/P_a)^{1/3}$ and the initial radius of superheated volume of liquid $r_0 = (3M/4\pi\rho_0)^{1/3}$ are proportional to a constant factor. Therefore, the problem can be reduced to non-dimensional variables in which the equations, together with the initial and boundary conditions, are scaled exactly and are independent of the liquid mass M.

To elucidate this similarity, in Fig. 10*a* the pressure profiles calculated for propane explosions at the initial pressure $P_0 = 10$ bar are shown; the solid lines are obtained for the vessel diameter of $D = 1$ m, while dots represent the solutions obtained for $D = 0.2$ and 4 m. For each set of initial conditions, pressure profiles are shown at three instants corresponding to non-dimensional times $\bar{t} = tU_*/r_* = 5.55 \cdot 10^{-2}$, $2.78 \cdot 10^{-1}$, and $5.55 \cdot 10^{-1}$. For $P_0 = 10$ bar, the characteristic expansion velocity is $U_* = 216.4$ m/s; for the small vessel ($D = 0.2$ m) we have the energy-based radius is $r_* = 0.78$ m, the dimensional times on the graphs are $t = 0.2$, 1, and 2 ms; for the medium-size vessel ($D = 1$ m) $r_* = 3.90$ m, the dimensional times are $t = 1$, 5, and 10 ms; whereas for the large vessel ($D = 4$ m) $r_* = 15.6$ m and $t = 4$, 20, and 40 ms.

Similar results obtained for $P_0 = 20$ bar are plotted in Fig. 10*b* at three non-dimensional times $\bar{t} = tU_*/r_* = 6.53 \cdot 10^{-2}$, $3.27 \cdot 10^{-1}$, and $6.53 \cdot 10^{-1}$. For this initial conditions, the characteristic expansion velocity is $U_* = 312.4$ m/s; for the small vessel ($D = 0.2$ m) $r_* = 0.96$ m, the dimensional times are $t = 0.2$, 1, and 2 ms; for the medium-size vessel ($D = 1$ m) $r_* = 4.78$ m, $t = 1$, 5, and 10 ms; whereas for the large vessel ($D = 4$ m) $r_* = 19.1$ m, $t = 4$, 20, and 40 ms.

One can see that all corresponding pressure profiles coincide, which confirms the similarity of solutions. Due to this

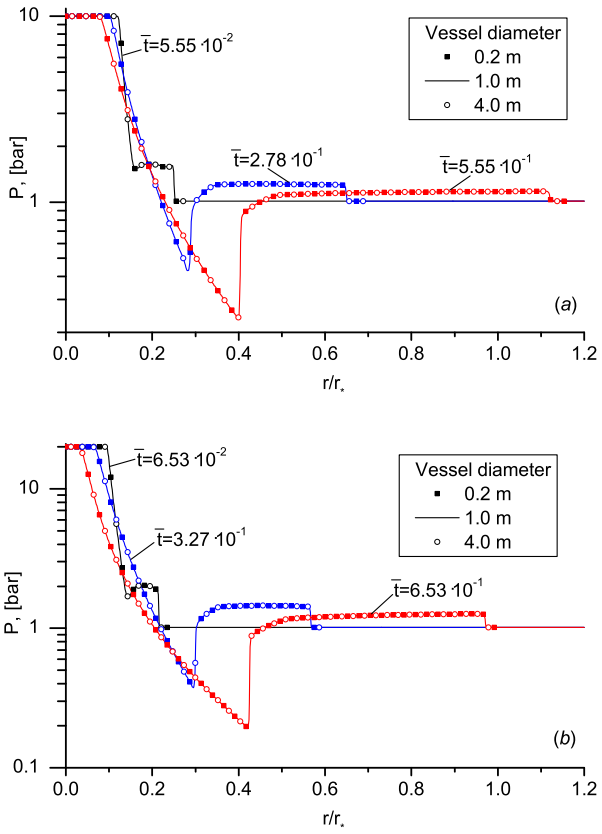

Figure 10: Pressure profiles from expansion of superheated propane clouds with different initial masses: (*a*) $P_0 = 10$ bar; (*b*) $P_0 = 20$ bar.

similarity, it is sufficient to carry on further studies just for one fixed mass of substance.

5.3.2. *Effect of initial pressure*

We consider here explosions of pressure-liquefied propane contained in the vessel of diameter $D = 1$ m, with the initial pressure varied in the range $P_0 = 5 - 30$ bar. The lower boundary corresponds to $T_0 = 275.3$ K (subcooled with respect to the ambient temperature $T_a = 298$ K), at the upper boundary $T_0 = 351.5$ K (preheated substance), the density decreasing from $\rho_0 = 526.3$ to 381.1 kg/m^3; the initial mass in the fixed-volume vessel decreasing from 276 to 200 kg. The specific energy yields range from 9.61 to 73.3 kJ/kg which gives r_* between 3.0 and 5.3 m; the ratio of initial radius of the cloud and the energy-based radius ranges between $r_0/r_* = 0.167$ and 0.094. Variation of initial pressure leads to variation in the pressure ratio P_0/P_a, density ratio ρ_0/ρ_a, and affects the sound of speed in the two-phase mixture, see Fig. 3. As a result, no full similarity of the solutions can be expected. The task is, therefore, to evaluate the maximum overpressure as a function of initial state of the cloud for different initial states.

When comparing the overpressure-distance curves from BLEVEs with those of TNT explosions, it should be taken into account that TNT curves are normally given for near-surface explosions, while simulations were carried out for spherically symmetric physical explosions in an unbounded atmosphere. A common approach is to double the energy yields when calculating the energy-based radius because the blast wave propagates into half-space. Therefore, we consider here the energy-based radius $\hat{r}_* = (2E/P_a)^{1/3}$, where E is the energy yield. The results are presented in Fig. 11, together with the TNT curve [32]:

$$\frac{\Delta P}{P_a} = \frac{808\left[1+\left(\frac{Z}{4.5}\right)^2\right]}{\sqrt{1+\left(\frac{Z}{0.048}\right)^2}\sqrt{1+\left(\frac{Z}{0.32}\right)^2}\sqrt{1+\left(\frac{Z}{1.35}\right)^2}} \qquad (11)$$

Here, $Z = r/m_{TNT}^{1/3}$ is the normalized distance converted to non-dimensional radius by $r/\hat{r}_* = Z(P_a/W_{TNT})^{1/3}$, with $W = 4.184$ MJ/kg.

The results presented in Fig. 11 confirm that blast waves from BLEVEs are weaker than those of high explosives. The difference is especially notable for low initial pressures (5 and 10 bar), when the characteristic expansion velocities are below the speed of sound in air (see Table 1).

5.4. *Comparison with shock tube flows and compressed gas explosions*

Bursts of vessels containing pressurized non-condensable gases also fall into the category of "physical" explosions, therefore, it is interesting to compare the predicted characteristics of BLEVE blast waves with those of compressed gas explosions. Blast waves from compressed gas explosions were studied experimentally [33, 12] and numerically [34, 13].

From the gas dynamics point of view, flows at the initial stage of explosions of both types are described by the classical Riemann problem on the flows generated by an initial discontinuity separating two gas domains of high and low pressure with zero initial velocities. Breaking of a diaphragm (in a shock tube) or pressurized vessel failure initiates propagation of a shock wave into the low-pressure domain followed by the moving contact surface, while a rarefaction wave propagates into the high-pressure gas causing gradual pressure equalization in the system. In the planar one-dimensional case, the pressure and velocity between the leading shock and trailing contact surface are constant, they are described by the well-known shock tube formulas relating the initial pressure ratio P_0/P_a to the shock Mach number, M_S, and relative shock amplitude, P_{ST}/P_a. In the case of compressed air with the same initial temperature as the ambient atmosphere (i. e., the ratios of specific heats γ and speeds of sound are the same in the low and high-pressure domains), the shock tube formulas take the form

$$\begin{aligned}
\frac{P_{ST}}{P_a} &= 1 + \frac{2\gamma}{\gamma+1}\left(M_S^2 - 1\right) \\
\frac{P_0}{P_a} &= \frac{P_{ST}}{P_a}\left[1 - \frac{\gamma-1}{\gamma+1}\left(M_S - \frac{1}{M_S}\right)\right]^{-\frac{2\gamma}{\gamma-1}} \\
U_{ST} &= M_S c_{s0}\left(1 - \frac{2+(\gamma-1)M_S^2}{(\gamma+1)M_S^2}\right)
\end{aligned} \qquad (12)$$

where U_{ST} is the absolute gas velocity behind the traveling shock, $c_{s0} = \sqrt{\gamma P_a/\rho_a}$ is the sound speed in atmospheric air.

In the case of compressed gas explosions, as opposed to shock tube flow, blast wave amplitude decreases with distance. However, at small distances the geometry effects are still weak, and the initial amplitude of shock wave near the discontinuity can be evaluated from the shock tube relations (12). Evidently, these formulas are not applicable to BLEVEs due to the substance on high-pressure side of discontinuity being differ-

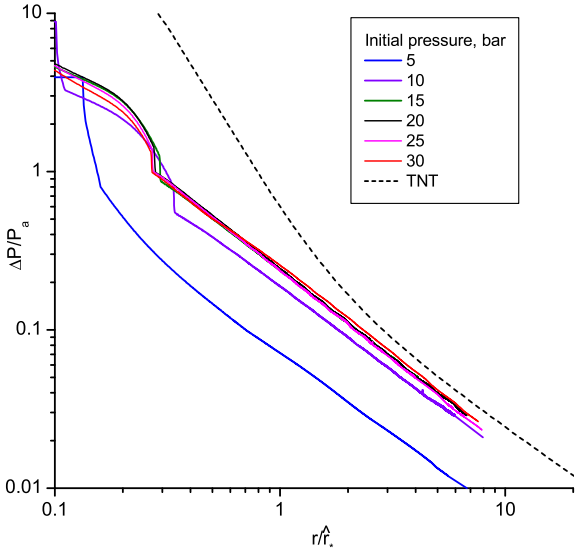

Figure 11: Scaled overpressure-distance curves for liquified propane explosions, in comparison with TNT curve [32]

Table 3: Initial blast wave pressure P_S and contact surface velocity U_C for shock tube, compressed gas explosions, and BLEVEs

P_0	Shock tube			Compressed air			Propane BLEVE		
	M_S	P_{ST}	U_{ST}	P_S	U_C	$\bar{r}_0$	P_S	U_C	$\bar{r}_0$
5	1.40	2.14	216.7	2.11	194	0.375	1.53	117	0.168
10	1.60	2.87	280.0	2.82	278	0.272	2.01	186	0.128
15	1.73	3.37	329.4	3.25	329	0.229	2.36	233	0.113
20	1.82	3.76	364.2	3.65	358	0.203	2.70	280	0.104
25	1.90	4.08	391.1	3.95	385	0.186	3.05	314	0.099
30	1.96	4.36	413.1	4.23	408	0.173	3.35	344	0.095
50	2.13	5.19	474.2	5.10	467	0.142	—	—	—
100	2.37	6.54	555.5	6.40	550	0.110	—	—	—

ent from compressed air. Therefore, it is of interest to compare in more detail the Riemann problem solutions for shock tube (1D linear geometry), compressed gas (spherical geometry), and BLEVE. To this end, a set of simulations was run for bursts of a spherical vessel of 1 m diameter, filled with air compressed to pressure P_0 = 5–100 bar, as well as for propane BLEVEs. In order to provide detailed data on blast waves straight after vessel burst, these simulations were run on a grid spanning the radius 0–5 m, with 10^4 cells (i. e., the cell size was 0.5 mm, ten times smaller than in Section 5.1).

In Fig. 12 and 13, pressure and velocity profiles obtained during the first 0.2 ms of compressed gas explosion and propane BLEVE are plotted; in both cases the initial pressure in the vessel was P_0 = 20 bar. The round symbols on each graph denote the position of contact surface, the shock tube solutions obtained from Eq. (12) are shown by the horizontal dashed lines. One can see that on the initial interval, lasting approximately for 0.05 ms, the pressure and velocity of the contact surface are nearly constant, after which both decay with time gradually. The initial contact surface velocity, U_C, and pressure, P_C, were estimated as average values over the first four time instants shown; the corresponding levels are shown by the dotted lines.

The data presented in Fig. 12 and 13 clearly show that the blast wave generated by compressed gas explosion is very well reproduced by the shock tube formulas, which is expected, or course. Comparing the compressed gas explosion with BLEVE, we see that in the latter case the shock wave amplitude and velocity are lower. It is also evident that the rarefaction wave propagates into the two-phase mixture much slower, traveling the distance of just 1 cm over the time 0.2 ms, as opposed to 7.5 cm traveled by the rarefaction wave in compressed air. This result confirms the reasoning of the low speed of sound in two-phase mixture being the limiting factor for energy release rate in BLEVEs (see Section 4).

To further elucidate the differences between the compressed gas explosions and BLEVEs, in Table 3 the shock tube parameters (exact Riemann problem solution for M_S, P_{ST}, U_{ST}) are listed in the wide range of initial pressures, together with the contact surface pressure P_C and velocity U_C obtained numerically for compressed gas explosions and BLEVEs (all pressures are given in bars, velocities in meters per second). Evidently, in the two-phase case the shock waves generated by the same pressure ratio are weaker than those of compressed air explosions.

Compare now the properties of shock waves from com-

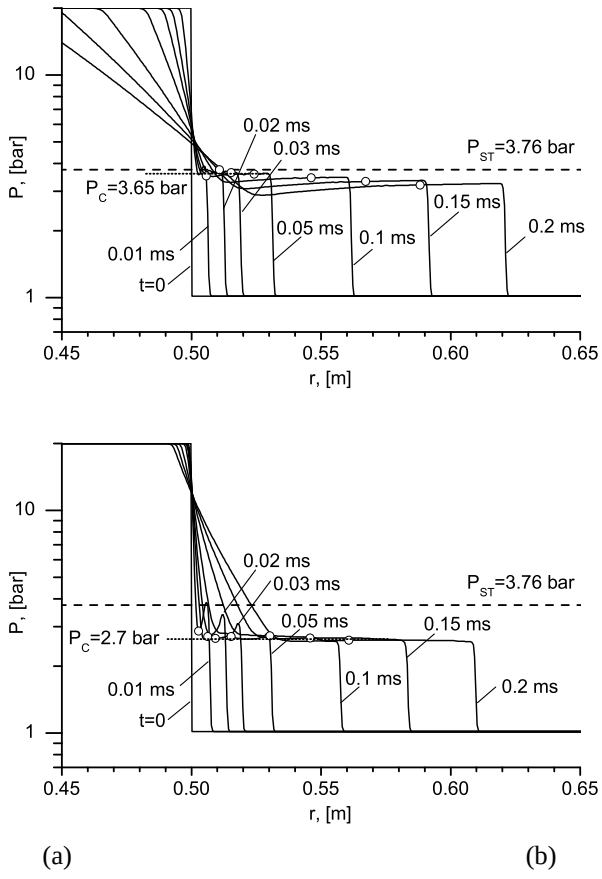

Figure 12: Shock wave formation in physical explosions at P_0 = 20 bar: (*a*) compressed air; (*b*) propane BLEVE.

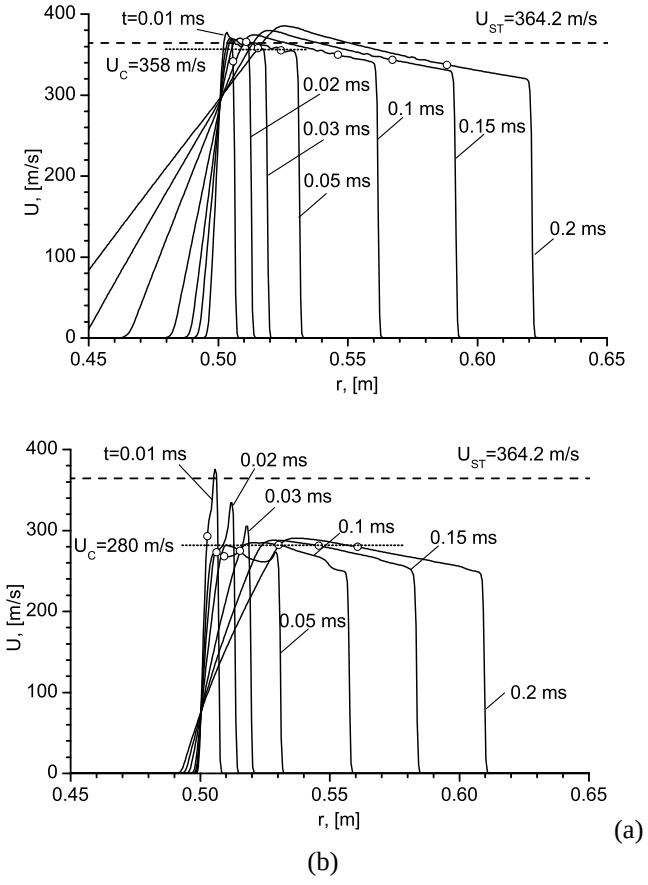

Figure 13: Velocity profiles in physical explosions at $P_0 = 20$ bar: (*a*) compressed air; (*b*) propane BLEVE.

pressed gas explosions and BLEVEs at larger distances from the source. A known feature of Riemann problem solutions is that the shock wave pressure P_{ST} is significantly lower than the driving pressure P_0 (see the first and third columns in Table 3), which limits the maximum attainable blast wave overpressures. For example, compressed gas explosion with the initial pressure as high as 100 bar generates a blast wave with initial relative overpressure $\overline{\Delta P} = (P_S - P_a)/P_a = 5.45$; for propane BLEVEs with vessel pressure of 30 bar the blast wave overpressure is as low as 2.31. However, when comparing the blast wave properties with those of high explosives, one need to take into account not only the overpressure *per se*, but also the scaled distances at which these overpressures are attained. It is only the "distance–overpressure" combination that provides meaningful comparison and evaluation of blast wave hazards.

The energy released in pressurized gas explosion can be evaluated from the adiabatic expansion work [35]:

$$E = \frac{P_0 V}{\gamma - 1}\left(1 - \left(\frac{P_0}{P_a}\right)^{\frac{\gamma-1}{\gamma}}\right) \tag{13}$$

where $V = 4\pi r_0^3/3$ is the vessel volume. The non-dimensional distance at which the shock wave is formed just after the vessel burst can be evaluated as $\bar{r}_0 = r_0 (P_a/E)^{1/3}$. For BLEVEs, the same procedure can be applied, with the energy yield evaluated from isoentropic relations, see Section 5.3.1. The resulting values of $\bar{r}_0$ are shown in Table 3 (note that $\bar{r}_0$ does not depend on vessel size, it is determined by the energy density normalized by the ambient pressure). Comparison shows that for any initial vessel pressure, two-phase explosions are characterized by lower initial overpressures attained at shorter non-dimensional distances. This shows that efficiency of energy release in BLEVEs is inferior to that in pressurized gas explosions.

Finally, compare the overpressure-scaled distance curves for pressurized gas explosions with TNT curves. In Fig. 14, results of numerical simulations are presented. Also shown are two approximations for TNT (see [32, 34]): i) Eq. (11), and ii) Warren's formula $\overline{\Delta P} = 0.6(r_*/r)^{4/3}$; note that their predictions are quite consistent at in the far zone, but deviate in the near zone. By points in Fig. 14 the experimental data [12] are plotted. An important reservation must be made on the data in Fig. 14: since the experiments [12] were performed for spherical glass spheres raised above the ground, no shock wave reflection from the ground occurred, and, therefore, the length scale was defined without doubling the energy yield (as opposed to Fig. 11). For TNT approximation (11), this was achieved by reducing the argument by a factor $2^{1/3} = 1.26$. Another important issue not to be overlooked is that in the original experimental work [12], the yield of pressurized gas explosion was defined as $E = (P_0 - P_a)V/(\gamma - 1)$, which gives higher values than the isoentropic formula (13) adopted here. Also, the pressure P_0 entering this definition is not the initial one, but some effective value evaluated by subtracting the kinetic energy of shattered wall fragments. For consistency, when plotting the experimental points in Fig. 14, the energy-based radius r_* was recalculated by the same procedure as described in [12], however, with en-

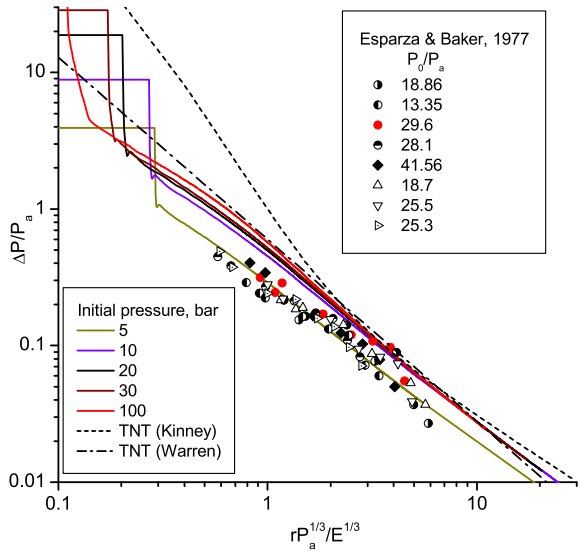

Figure 14: Scaled overpressure-distance curves for pressurized air, in comparison with experiments [12] and TNT curves [32]

ergy E evaluated from (13). As a result, the non-dimensional radii given in [12] were multiplied by a factor of approximately 1.2.

It follows from Fig 14 that simulations predict somewhat higher overpressures than those measured experimentally, the fact also mentioned in the original work [12]. Importantly, however, the overpressure scales primarily with the reduce distance, and much weaker depends in the far zone on the initial pressure. Overall, the numerical solutions obtained agree well with the results [34] where more detailed analysis of pressurized gas explosions can be found.

5.5. 2D simulations of near-ground BLEVEs and validation against experiments

Consider now results of two-dimensional (axisymmetric) simulations of near-surface BLEVEs aimed at validation of the model developed in this paper against field tests [7, 8]. This experimental series still remains one of the most representative because of the wide range of pressure-liquefied gas (propylene) masses studied, M = 0.125–452 kg. Another reason for choosing these experiments is that the vessel was filled with liquefied gas completely, which agrees with the assumption of all-liquid initial state (see the left-hand side of Eq. (4)). In the experiments, the vessel was preheated, so that the initial pressure reached P_0 = 40 atm. Vessel burst was initiated by detonating a small TNT charge, providing nearly instantaneous loss of containment, a condition also assumed in the current model.

In Figs. 15 and 16, simulation results for the largest mass M = 452 kg of propylene from tests [7, 8] are presented at the instants 1, 3, 5, and 7 ms. The pressure fields shown in the top row demonstrate the formation of blast wave in the atmosphere, its reflection from the ground surface and propagation along it. The bottom row demonstrates expansion of the two-phase zone which acts as a “piston” for pressure wave development in the atmosphere.

Figs. 15 and 16 show that during the first 5 ms a minimum of x_v persists in the central area of the cloud where high pressure is maintained. As was discussed above (see Section 5.1), this shows that boil-up of superheated liquid does not occur simultaneously over the whole volume. Rather, it occurs in the boil-up wave propagating through the superheated liquid at a finite velocity limited by the low speed of sound on its two-phase side. By the time t = 7 ms, whole volume of liquid is boiling, and maximum pressure drops from its initial value.

A series of numerical simulations was carried out for the same masses of propylene as in experiments [7, 8] (0.125, 1.6, 12.8, 452 kg). In order to compare the results obtained with the field test data, the maximum overpressures recorded in simulations at various distances are plotted in Fig. 17 together with the experimental results. As the abscissa, the distance divided by the cubic root of mass, $r/M^{1/3}$, is used, in accordance with the way the results were presented in [7, 8]. Since all experiments [7, 8] were performed at the same initial conditions, i. e., the specific blast yield Δh_{lv} (see Eq. (9)) is constant in all cases, this is equivalent to normalization of distance by the energy-based scale $(E/P_0)^{1/3}$.

The results presented in Fig. 17 show that the model developed in this work describes adequately the gas dynamics effects of BLEVEs. Notably, all curves merge in the far zone to a single line, while in the near zone differences are observed because the initial height of the superheated liquid volume was kept constant in the simulations, i. e., it does not scale with the explosion energy.

Another way to compare the simulation results with experimental data is taken in Fig. 18 where for each point the abscissa is equal to the maximum overpressure obtained in simulations, the ordinate is the corresponding experimental measurement (so-called parity plot). The diagonal shown by the dashed line denotes ideal agreement of simulations and experiments, whereas the scatter and bias characterize the discrepancy. One can see that no systematic bias is observed, thus the agreement is adequate, keeping in mind that experimental results on BLEVEs are quite “noisy”.

It is important to note that agreement between the simulated results and experimental data was obtained without any calibration of model parameters (in fact, there are no adjustable parameters in the model at all!). At the same time, the model involves quite “rich” data on the substance because it essentially includes substance-specific properties (pressure, temperature, phase densities, specific enthalpies and entropies) on the saturation line.

6. Conclusions

It is important to note that low efficiency of physical explosions in comparison with TNT was demonstrated in this work assuming that i) there are no irreversible energy losses in the mixture, and ii) boiling/condensation occur instantaneously, and

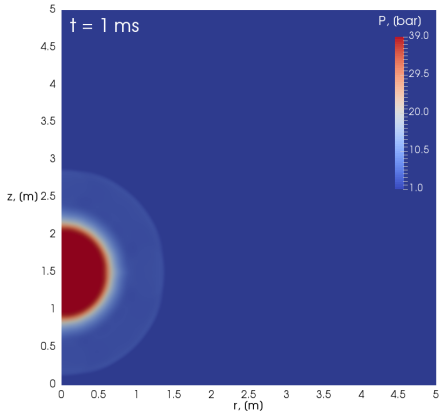

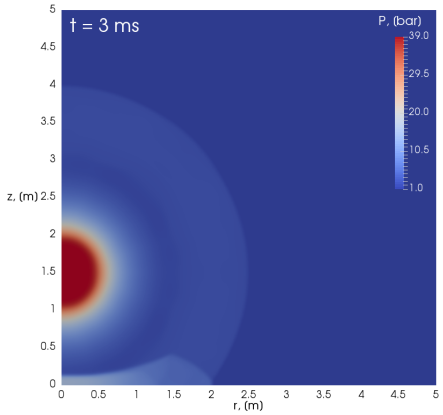

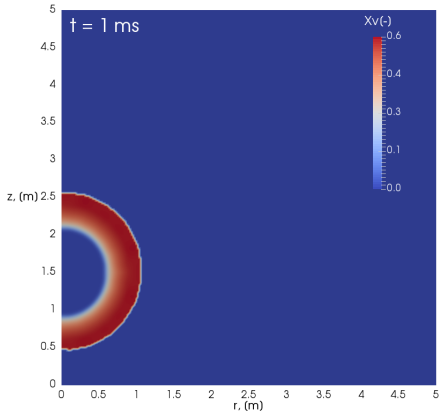

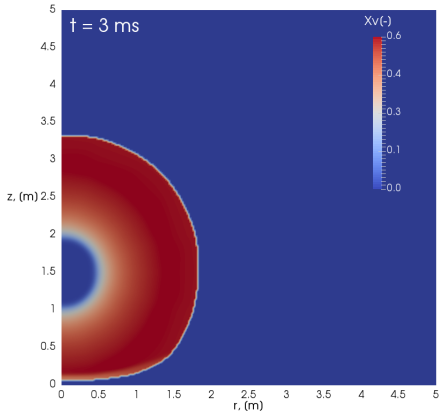

Figure 15: Pressure (top row) and mass fraction of vapor (bottom row) fields upon near-surface burst of 452 kg of propylene

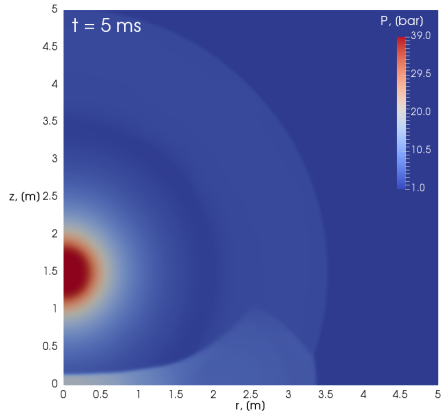

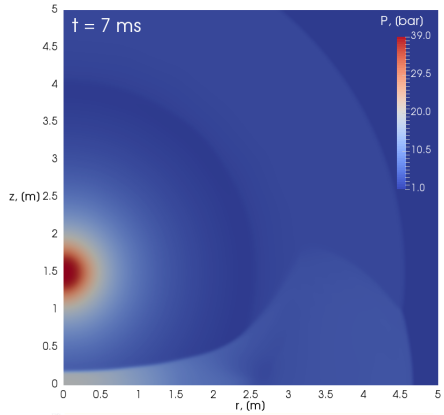

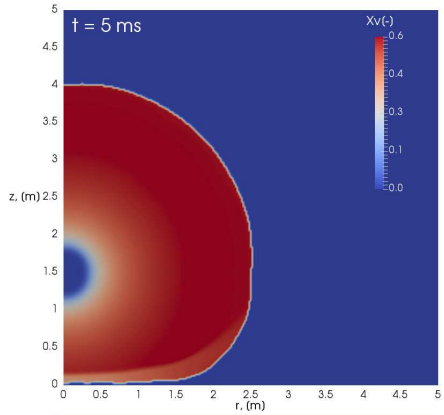

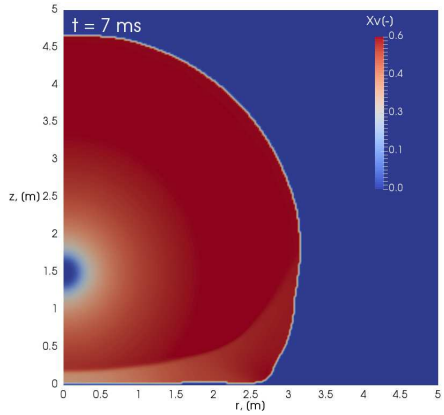

Figure 16: Pressure (top row) and mass fraction of vapor (bottom row) fields upon near-surface burst of 452 kg of propylene (*continued*)

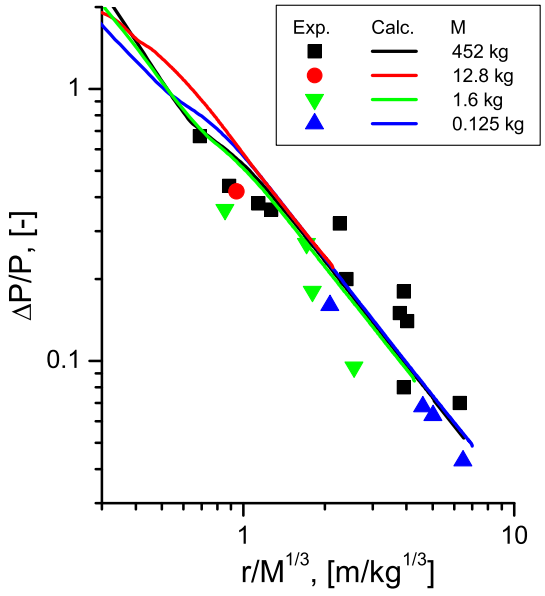

Figure 17: Overpressure from BLEVEs: simulations (lines) vs experiments (dots).

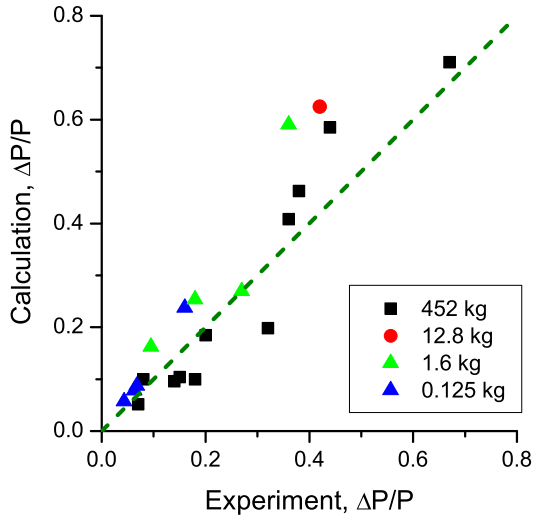

Figure 18: Overpressure from BLEVEs: simulations (horiz.) vs experiments (vert.).

the phase transition rate is not limited by non-equilibrium processes at the vapor/liquid interface. Even in these idealized conditions, the blast wave overpressures obtained are lower than those from detonation of high explosives. The physical reason that BLEVE blast waves are weaker lies not in the energy being lost irreversibly, but in the fact that the cloud boils up over a finite time, which makes it a less efficient "piston" for generation of blast waves due to energy release rate being limited by propagation of boiling wave through the bulk of superheated liquid. In this respect, boiling up of superheated liquid is expansion-controlled, but rather than occurring uniformly over the whole volume, it proceeds "layer-by-layer". In our view, the physical mechanisms determining the blast effects of BLEVEs revealed in this paper are more significant than fine details on bubble nucleation, growth etc [22]. This must be especially true in safety applications, where the time scales related to two-phase cloud expansion are much longer (due to large size of the system) that the time scales of microscopic processes around individual bubbles.

Simulations of single-phase flows relevant to pressurized gas explosions indicated that in this case the blast wave overpressures are higher than those of BLEVEs with the same preburst pressure. It should be kept in mind, however, that superheated liquids possess much higher energy density: for example, for the initial pressure $P_0 = 25$ bar and vessel diameter 1 m, the energy release in pressurized gas explosion is 2 MJ, while in propane BLEVE the yield is 13 MJ, which by far offsets the difference in explosion efficiencies.

Simulations revealed the multi-shock structure of BLEVE blast waves in the conditions where no vapor was present initially in the vessel (all-liquid initial state). The physical reason for the occurrence of secondary shocks is overexpansion of the two-phase cloud followed by development of a converging shock imploding at the cloud center, the sequence of events known for expansion of pressurized gas clouds. Therefore, more careful analysis must be taken in identification of the reasons for multiple-shock pressure records observed experimentally (e.g., in [10] it is argued that vapor expansion can be responsible for the pressure peaks, while flashing is too slow a process to contribute significantly).

Further work, requiring some (quite straightforward, though) extension of model formulation and implementation is to consider the mass fraction of vapor x_v in the initial state not as zero throughout the volume (all-liquid assumption), but as a function of spatial coordinates. This would allow us to analyze BLEVEs of partially filled containers necessary to validate the model against available such experiments [9, 10, 19] and clarify the relative input of expanding vapor space and flashing liquid into the BLEVE blast wave. Also, effects of vessel shape (sphere, cylinder) can also be evaluated and compared with experimental data.

References

[1] V. Marshall, Major Chemical Hazards, Ellis-Horwood, Chichester, UK, 1987.

[2] B. E. Gelfand, Features and simulations of non-ideal explosions, in: Proceedings of the 3rd Int. Seminar on Fire and Explosion Hazards, University of Central Lancashire, Preston, Lancs, 2001, pp. 43–56.

[3] CCPS (Center for Chemical Process Safety), Guidelines for Vapor Cloud Explosion, Pressure Vessel Burst, BLEVE and Flash Fire Hazards, 2nd Edition, Wiley, 2010.

[4] T. Abbasi, S. A. Abbasi, The boiling liquid expanding vapour explosion (BLEVE): Mechanism, consequence assessment, management, Journal of Hazardous Materials 141 (2007) 489–519. doi:10.1016/j.jhazmat.2006.09.056.

[5] B. E. Gel'fand, S. P. Medvedev, A. N. Polenov, S. M. Frolov, Shock waves in the dispersal of liquid-saturated vapor systems, High Temperature 27 (6) (1989) 923–930.

[6] S. P. Medvedev, A. N. Polenov, B. E. Gel'fand, Shock-wave parameters in the explosive expansion of effervescing liquid, Combustion, Explosion and Shock Waves 27 (4) (1991) 438–442. doi:10.1007/BF00789555.

[7] H. Giesbrecht, K. Hess, W. Leuckel, B. Maurer, Analysis of explosion hazards on spontaneous release of inflammable gases into the atmosphere. Part 1: Propagation and deflagration of vapour clouds on the basis of bursting tests on model vessels, Ger. Chem. Eng. 4 (1981) 305–314.

[8] H. Giesbrecht, G. Hemmer, K. Hess, W. Leuckel, A. Stoeckel, Analysis of explosion hazards on spontaneous release of inflammable gases into the atmosphere. Part 2: Comparison of explosion model derived from experiments with damage effects of explosion accidents, Ger. Chem. Eng. 4 (1981) 315–325.

[9] A. M. Birk, M. H. Cunningham, Liquid temperature stratification and its effect on BLEVEs and their hazards, Journal of Hazardous Materials 48 (1-3) (1996) 219–237. doi:10.1016/0304-3894(95)00157-3.

[10] A. M. Birk, C. Davison, M. Cunningham, Blast overpressures from medium scale BLEVE tests, Journal of Loss Prevention in the Process Industries 20 (3) (2007) 194–206. doi:10.1016/j.jlp.2007.03.001.

[11] E. D. Esparza, W. E. Baker, Measurements of blast waves from bursting frangible spheres pressurized with flash-evaporating vapor or liquid, Tech. Rep. CR-2811, NASA (1977).

[12] E. D. Esparza, W. E. Baker, Measurement of blast waves from bursting pressurized frangible spheres, Tech. Rep. CR-2843, NASA (1977).

[13] G. M. Makhviladze, S. E. Yakush, Blast waves and fireballs from bursts of vessels with pressure-liquefied hydrocarbons, Proceedings of the Combustion Institute 29 (1) (2002) 313–320. doi:10.1016/S1540-7489(02)80042-6.

[14] G. M. Makhviladze, S. E. Yakush, Modelling of formation and combustion of accidentally released fuel clouds, Process Safety and Environmental Protection 83 (2) (2005) 171–177. doi:10.1205/psep.04242.

[15] S. E. Yakush, Expansion of high-pressure superheated liquids: multiphase flows and shock effects, in: Proc. 7th International Symposium on Turbulence, Heat and Mass Transfer, Palermo, Italy, 24-27 Sept. 2012, Begell House Inc., New York, Wallingford, 2012, pp. 937–940.

[16] A. C. van den Berg, M. M. van der Voort, J. Weerheijm, N. H. A. Versloot, Expansion-controlled evaporation: A safe approach to BLEVE blast, Journal of Loss Prevention in the Process Industries 17 (6) (2004) 397–405. doi:10.1016/j.jlp.2004.07.002.

[17] M. M. van der Voort, A. C. van den Berg, D. J. E. M. Roekaerts, M. Xie, P. C. J. de Bruijn, Blast from explosive evaporation of carbon dioxide: Experiment, modeling and physics, Shock Waves 22 (2) (2012) 129–140. doi:10.1007/s00193-012-0356-0.

[18] D. Laboureur, F. Heymes, E. Lapebie, J. M. Buchlin, P. Rambaud, BLEVE overpressure: Multiscale comparison of blast wave modeling, Process Safety Progress 33 (3) (2014) 274–284. doi:10.1002/prs.11626.

[19] D. Laboureur, A. M. Birk, J. M. Buchlin, P. Rambaud, L. Aprin, F. Heymes, A. Osmont, A closer look at BLEVE overpressure, Process Safety and Environmental Protection 95 (0) (2015) 159–171. doi:http://dx.doi.org/10.1016/j.psep.2015.03.004.

[20] E. Planas-Cuchi, J. M. Salla, J. Casal, Calculating overpressure from BLEVE explosions, Journal of Loss Prevention in the Process Industries 17 (6) (2004) 431–436. doi:10.1016/j.jlp.2004.08.002.

[21] T. Abbasi, S. A. Abbasi, Accidental risk of superheated liquids and a framework for predicting the superheat limit, Journal of Loss Prevention in the Process Industries 20 (2) (2007) 165–181. doi:10.1016/j.jlp.2005.11.002.

[22] G. A. Pinhasi, A. Ullmann, A. Dayan, 1D plane numerical model for boiling liquid expanding vapor explosion (BLEVE), International Journal of Heat and Mass Transfer 50 (23-24) (2007) 4780–4795. doi:10.1016/j.ijheatmasstransfer.2007.03.016.

[23] J. M. Salla, M. Demichela, J. Casal, BLEVE: A new approach to the superheat limit temperature, Journal of Loss Prevention in the Process Industries 19 (6) (2006) 690–700. doi:10.1016/j.jlp.2006.04.004.

[24] J. Casal, J. M. Salla, Using liquid superheating energy for a quick estimation of overpressure in BLEVEs and similar explosions, Journal of Hazardous Materials 137 (3) (2006) 1321–1327. doi:10.1016/j.jhazmat.2006.05.001.

[25] R. I. Nigmatulin, J. C. Friedly, Dynamics of Multiphase Media. Vol. 1 and 2, CRC Press, 1990.

[26] J. R. Macdonald, Some Simple Isothermal Equations of State, Reviews of Modern Physics 38 (4) (1966) 669–679. doi:10.1103/RevModPhys.38.669.

[27] R. P. Fedkiw, T. Aslam, B. Merriman, S. Osher, A non-oscillatory Eulerian approach to interfaces in multimaterial flows (the Ghost Fluid Method), Journal of Computational Physics 152 (2) (1999) 457–492. doi:10.1006/jcph.1999.6236.

[28] S. Osher, R. P. Fedkiw, The Level Set Methods and Dynamic Implicit Surfaces, Springer-Verlag, 2002.

[29] A. Kurganov, E. Tadmor, New high-resolution central schemes for nonlinear conservation laws and convection-diffusion equations, Journal of Computational Physics 160 (1) (2000) 241–282. doi:http://dx.doi.org/10.1006/jcph.2000.6459.

[30] NIST Chemistry Webbook, http://webbook.nist.gov/chemistry/fluid.

[31] H. Miyamoto, K. Watanabe, A Thermodynamic Property Model for Fluid-Phase Propane, International Journal of Thermophysics 21 (5) (2000) 3–14. doi:10.1023/A:1026441903474.

[32] G. Kinney, K. Graham, Explosive Shocks in Air, 2nd Edition, Springer, 1985. doi:10.1007/978-3-642-86682-1.

[33] D. W. Boyer, An experimental study of the explosion generated by a pressurized sphere, Journal of Fluid Mechanics 9 (1960) 401–429. doi:10.1017/S0022112060001195.

[34] B. Vanderstraeten, M. Lefebvre, J. Berghmans, Simple blast wave model for bursting spheres based on numerical simulation, Journal of Hazardous Materials 46 (2-3) (1996) 145–157. doi:10.1016/0304-3894(95)00066-6.

[35] W. Baker, P. A. Cox, P. S. Westine, J. J. Kulesz, R. A. Strehlow, Explosion Hazards and Evaluation, Elsevier B.V., Amsterdam, 1983.